CrossMark

North Pacific decadal variability in the CMIP5 last millennium simulations

Laura E. Fleming[1,2] · Kevin J. Anchukaitis[1,3]

Abstract The Pacific ocean–atmosphere system exerts an important influence on the climate of Asia and North America, but the limited length of the observational record prevents a complete understanding of its bidecadal and multidecadal time scales. Paleoclimate reconstructions provide one source of information on longer time scales, although they differ in their estimation of the behavior of the Pacific decadal oscillation (PDO) prior to the instrumental period. Forced general circulation model simulations offer complementary long-term perspectives on both the history and dynamics of this important mode of variability. Here, we analyze the PDO in the ensemble of CMIP5/PMIP3 last millennium (past1000 + historical) simulations. We evaluate the modeled spatial, temporal, and spectral characteristics of this mode, as well as teleconnections between North Pacific variability and global climate. All models produce a mode of North Pacific variability over the last millennium with spatial patterns and spectral power density similar to observations. CCSM, FGOALS, and IPSL best reproduce observed spatial patterns, spectral characteristics, and teleconnections to terrestrial regions used in paleoclimate proxy reconstructions. In these simulations, the PDO shows no consistent response to solar or volcanic forcing.

Keywords Decadal · Pacific · PDO · General circulation models · CMIP5 · Last millennium

✉ Kevin J. Anchukaitis
kanchukaitis@email.arizona.edu

1   Department of Geology and Geophysics, Woods Hole
    Oceanographic Institution, Woods Hole, MA, USA

2   Joint Program in Oceanography/Applied Ocean Science
    and Engineering, Massachusetts Institute of Technology,
    Woods Hole Oceanographic Institution, Woods Hole, MA,
    USA

3   School of Geography and Development and Laboratory
    of Tree Ring Research, University of Arizona, Tucson, AZ,
    USA

1 Introduction

Decadal variability in the Pacific ocean–atmosphere system is an important feature of the global climate system. It influences regional temperature trends (Wang et al. 2009; Meehl et al. 2012; Weaver 2013; Deser et al. 2014) and is associated with plateaus in the rate of global surface temperature warming (e.g. Meehl et al. 2013; Brown et al. 2014). Decadal variability is associated with persistent hydroclimate anomalies over the adjacent continents (McCabe et al. 2004b; Gu and Adler 2012), and may therefore have both immediate and long-lasting consequences for society, infrastructure, and ecosystems (Keenlyside et al. 2008; Buckley et al. 2010; Swetnam and Betancourt 2010). However, our understanding of these decadal and multidecadal-scale ocean–atmosphere processes is restricted by both the long time scales of the phenomena and the limited length of the observational record, which also occurs entirely during an epoch of anthropogenic influence on the climate system. The Pacific decadal oscillation (PDO; Mantua et al. 1997; Zhang et al. 1997; Mantua and Hare 2002) is the leading mode of North Pacific sea surface temperatures (SST) and displays quasi-periodic bidecadal (10–30 years) and multidecadal (50–70 years) variability (Minobe 1997, 1999), and therefore instrumental observations at these time scales are extremely limited. The PDO appears to have experienced regime shifts

in 1925, 1947, 1977, and perhaps again in 1999 (Mantua et al. 1997; Peterson and Schwing 2003; Lyon et al. 2013), but early twentieth century variability appears to be reduced and less coherent than later in the century. McAfee (2014) demonstrated that observed winter PDO teleconnections to North American climate varies between these epoch, and St. George and Ault (2011) have shown that the magnitude and importance of decadal variability for winter rainfall along the central Pacific Coast of North America waxes and wanes over time. These observations and others (McCabe et al. 2004a; Wise 2014) suggest that the PDO may exhibit time-scale dependent or nonstationary behavior.

Proxy paleoclimate reconstructions of the PDO provide an opportunity to understand variability in its temporal and spectral characteristics—and its association with other components of the regional ocean–atmosphere circulation—prior to the epoch of significant potential anthropogenic influences. Reconstructions of Pacific decadal variability typically use corals and tree-rings (D'Arrigo et al. 2001; Evans et al. 2001a, b; Biondi et al. 2001; Gedalof and Smith 2001; D'Arrigo and Wilson 2006) to develop statistical estimates of the PDO index or spatiotemporal SST patterns in the past. These reconstructions differ from one another both temporally and spectrally (Gedalof et al. 2002; Evans et al. 2002; Kipfmueller et al. 2012; McAfee 2014; Wise 2014), however, and substantial uncertainty still exists about the stability, characteristic time scale, and stationarity of the PDO. Long general circulation model (GCM) paleoclimate simulations provide an additional, independent, and complementary source of information about the potential past and long-term behavior of North Pacific decadal variability and the extent of large-scale teleconnections to global and regional climate. GCMs evaluated as part of the Intergovernmental Panel on Climate Change (IPCC) reproduce decadal-scale ocean–atmosphere variability in the Pacific (Randall et al. 2007; Park et al. 2013), and the most recent Coupled Model Intercomparison Project Phase 5 (CMIP5; Taylor et al. 2012) included an experiment (past1000) to simulate the climate of the last millennium. It is now therefore possible to evaluate the long-term simulated Pacific decadal variability in an ensemble of transient, forced runs of state-of-the-art climate models, and to apply this understanding toward inferences concerning the potential range of past temporal and spectral variability in this mode.

Here, we evaluate North Pacific decadal and multidecadal variability within the ensemble of CMIP5 last millennium simulations. We compare the spatiotemporal variability in the models to that of observations, and analyze the spectrum of the simulated PDO in light of the presence and stability of modes of quasi-periodic decadal and multidecadal variability. We evaluate whether there is evidence for a coherent forced response of North Pacific variability to radiative forcing across the ensemble. We also observe the nature of simulated teleconnections from the North Pacific to global

patterns of temperature, precipitation, and sea level pressure. We consider these different lines of evidence in light of which models may provide optimal comparisons with proxy data and for use in pseudoproxy (e.g. Smerdon 2011) studies of PDO reconstruction data and methods. This work provides a necessary evaluation of climate model skill in simulating temporal, spatial, and spectral characteristic of the PDO prior to any subsequent comparison with proxies. It also provides insight into the potential long-term simulated behavior of this important mode of climate variability.

2 Data and methods

2.1 Model and observational data

Our model selection follows that of Bothe et al. (2013). We analyzed output from the following models from the Coupled Model Intercomparison Project Phase 5 (CMIP5; Taylor et al. 2012) for this study, for which there were completed and archived last millennium (past1000, 850–1850 CE; Schmidt et al. 2012) and historical simulations as of August 2013 (see Table 1): BCC (Xiao-Ge et al. 2012), CCSM4 (Landrum et al. 2013a), FGOALS (Zhou et al. 2011), GISS-R (Schmidt et al. 2014), IPSL-CM5A-LR (Dufresne et al. 2013), and MPI-ESM-P (Giorgetta et al. 2013). As in Bothe et al. (2013), we include only two of the eight past1000 members from the GISS ensemble (here R21 and R24), so as to not weigh the analysis unduly toward a single GCM. Due to drift in the GISS simulations, most apparent in the initial several centuries of the simulations, we excluded data from the years 850–1000 CE. We continued the simulations to the present (1850–1999 or 2005, depending on model) using historical simulations from the CMIP5 experiment. Most of our models have either continuous runs or matching historical simulations initialized from the end of the last millennium simulation. One notable exception is IPSL-CM5A-LR, which had no archived historical continuation at the time of this research. Despite this, there is no obvious discontinuity at the time scale examined here in the past1000+historical PDO calculated from the IPSL-CM5A-LR, nor do any of our analyses or conclusion herein, for IPSL or otherwise, depend on the extension of the simulations to the present. Following Knutson et al. (2013) we use the model surface ('skin') temperature field, which is available on regular grids, and following (Rayner et al. 2003) we set sea surface temperatures in regions covered with sea ice to $-1.8\,°C$, in order to be directly comparable with observations. In order to evaluate overall model performance, we additionally calculated and analyzed a multimodel Ensemble Mean by averaging climate fields across all ensemble members.

In order to compare the model simulated PDO to observations, we used gridded sea surface temperatures (SST)

Table 1 Selected climate models following Bothe et al. (2013) and their abbreviations, institute of origin, and the solar and volcanic forcing sets (Taylor et al. 2012; Schmidt et al. 2012)

Model (abbreviation)	Institute	Solar	Volcanic
BCC-CSM1-1 (BCC)	Beijing Climate Center China Meteorological Administration	Vieira et al. (2011)	Gao et al. (2008)
CCSM4	National Center for Atmospheric Research	Vieira et al. (2011)	Gao et al. (2008)
FGOALS-gl (FGOALS)	State Key Laboratory of Numerical Modeling for Atmospheric Sciences and Geophysical Fluid Dynamics, Institute of Atmospheric Physics, Chinese Academy of Sciences	Crowley (2000)	Crowley (2000)
GISS-E2-R (GISS-R21)	National Aeronautics and Space Administration, Goddard Institute for Space Studies	Steinhilber et al. (2009)	Crowley et al. (2008)
GISS-E2-R (GISS-R24)	National Aeronautics and Space Administration, Goddard Institute for Space Studies	Steinhilber et al. (2009)	Gao et al. (2008)
IPSL-CM5A-LR (IPSL)	Institut Pierre Simon Laplace	Vieira et al. (2011)	Gao et al. (2008)
MPI-ESM-P (MPI)	Max Planck Institute for Meteorology	Vieira et al. (2011)	Crowley et al. (2008)

from the UK Met Office Hadley Centre spanning 1870–2005 (HadISST; Rayner et al. 2003). This dataset estimates SSTs in data-sparse regions using a reduced space optimal interpolation of observations. The dataset comprises monthly mean fields on a $1° \times 1°$ grid. SST observations in the North Pacific are limited before the 1940s, and are particularly sparse prior to the twentieth century (Kaplan et al. 1998; Rayner et al. 2006; Deser et al. 2010). We also confirmed our analyses by additionally analyzing the observed PDO in the Extended Reconstructed Sea Surface Temperature (ERSST) dataset (v3b; Smith et al. 2008).

In order to evaluate observed against modeled PDO teleconnections, we use a set of three global gridded data products. We use sea level air pressure (SLP) observations from the NOAA-CIRES twentieth Century Reanalysis version 2 (20CRv2; Compo and Sardeshmukh 2006). This dataset is derived from observations of synoptic surface pressure, with boundary conditions from monthly SST and sea-ice distributions (Compo et al. 2011). The 20CRv2 dataset has monthly mean fields from 1871 to 2012 on a $2° \times 2°$ grid. We use precipitation observations from the GPCC Full Data Reanalysis Version 6.0 (Schneider et al. 2011). The GPCC dataset contains data from a large global set of land stations interpolated to optimize spatial coverage (Schneider et al. 2013). GPCC includes monthly mean fields from 1901 to 2010 on a $1° \times 1°$ grid. For surface temperature anomalies, we used the Goddard Institute for Space Studies (GISS) Surface Temperature Analysis (GISTEMP; Hansen et al. 2010). GISTEMP includes in situ meteorological station data and includes ERSST for sea surface temperature anomalies. These data are adjusted for non-climatic warming

trends in urban areas. GISTEMP comprises monthly mean fields from 1880 to 2014 on a $2° \times 2°$ grid.

2.2 Methods

For both observations and models, we calculated the PDO index as the leading mode from an empirical orthogonal function (EOF) analysis of monthly residual SST anomalies in the region 20°N–60°N, 110°E–110°W. We calculated the monthly mean anomalies by first removing the long-term monthly means and then subtracting the monthly mean global SST anomaly. Summer (winter) values are calculated as the mean of April though September (October through March). The EOF analysis yields spatial patterns (loadings) and temporal scores (time series).

In order to analyze the spectra of the observed and model simulated PDO, we performed a multitaper method (MTM) analysis (Thomson 1982) on the the seasonal indices, using bandwidth parameter $p = 2$ and $K = 3$ tapers. Statistical significance of narrow-band spectral peaks was estimated using a Monte Carlo simulation (n = 10,000) of first order autoregressive (AR1) red noise with coefficients estimated from the actual indices (Neumaier and Schneider 2001). We also determined a moving evolutive MTM using an 80-year moving-window incrementally advanced along the length of the time series (Priestley 1965).

In order to examine teleconnections between North Pacific and global climate, we computed the field correlation—the Pearson Product Moment Correlations between the PDO time series and every point in the respective field—for observations and modeled PDO indices in both

summer and winter against coeval precipitation, surface temperature, and sea level pressure fields. We also evaluated the lagged correlation between winter indices and summer climate fields, in order to observe whether knowledge of these teleconnections could allow for paleoclimate proxies reflecting local boreal summer or growing season conditions to be used to estimate the state of the prior winter PDO. Following Livezey and Chen (1983), we estimated the global (field) statistical significance of these correlations using a Monte Carlo simulation (n = 1000), reshuffling the field in time, recalculating the correlation with this randomized field, and counting the number of statistically significant correlations. If the original field correlation has more statistically significant correlations than the 95th percentile of the Monte Carlo correlations, then the original field correlation pattern were considered to be globally statistically significant (Livezey and Chen 1983).

3 Results

3.1 Spatiotemporal and spectral patterns

The spatial loading patterns of the leading EOF of North Pacific summer SST anomalies (the PDO) are shown in Fig. 1. Both models and observations show the characteristic 'horseshoe' spatial loading pattern, with negative loadings in the central North Pacific surrounded by positive anomalies in the Gulf of Alaska, the Bering Sea, and along the west coast of the United States extending toward the tropics. The spatial patterns of the leading mode of the winter EOF are shown in Fig. 2. CCSM, FGOALS, GISS, and IPSL are similar to observations, with negative loadings in most of the North

Pacific and positive loadings in the Bering Sea, the Gulf of Alaska, and off the west coast of the United States. Although the spatial patterns for BCC, MPI, and the Ensemble Mean are similar to the observations, the positive loadings extend throughout the tropical Pacific for these models. The spatial loadings for the ERSST dataset are almost identical in both summer and winter to the HadISST dataset (see Supplemental Materials), and therefore only the results from HadISST are discussed further.

Figure 3 shows annual and 21-year low pass filtered time series of the summer PDO index from models and observations, and the corresponding power spectra are shown in Fig. 5. All models display pronounced multidecadal variability; however, the spectra differ somewhat in their peak frequencies. FGOALS is the only model where the peak frequency of the spectrum is dominated by an interannual periodicity, at approximately 4 years (Fig. 4). The peak frequency for the Ensemble Mean occurs at about 15 years. The peak frequency for BCC occurs at about 20 years and for CCSM and MPI at about 40 years. Peak frequency for GISS R21 and IPSL occurs at about 65 years, while it occurs at somewhat longer wavelengths in GISS R24 (~90 years). The spectrum of the observed summer PDO shows maximum broadband power between approximately 30 and 65 years. Correlations between modeled and observed PDO indices are low, largely non-significant, and vary in sign (Table 2; $r = -0.20$ to 0.16).

Figure 4 shows annual and 21-year low pass filtered time series of the winter PDO index, with the power spectra shown in Fig. 6. As with the summer PDO index, all models display a pronounced multidecadal variability. The FGOALS spectrum is again dominated by interannual periodicity, with a maximum at approximately 4 years.
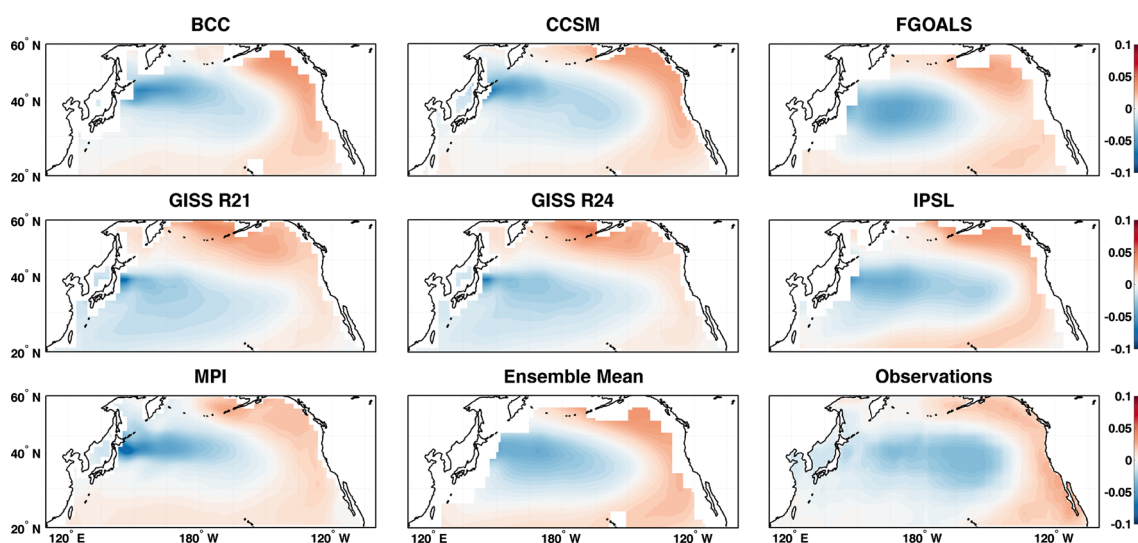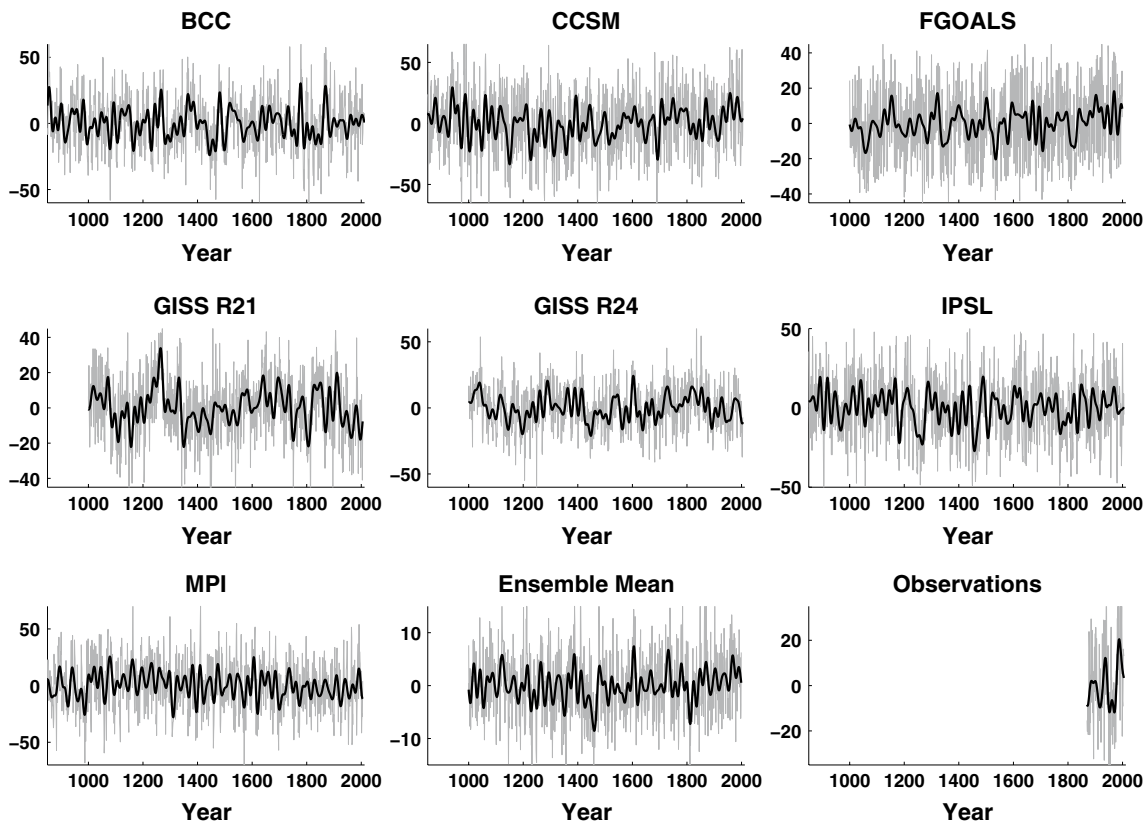

Fig. 1 Summer PDO loading pattern for simulations and observations (HadISST)
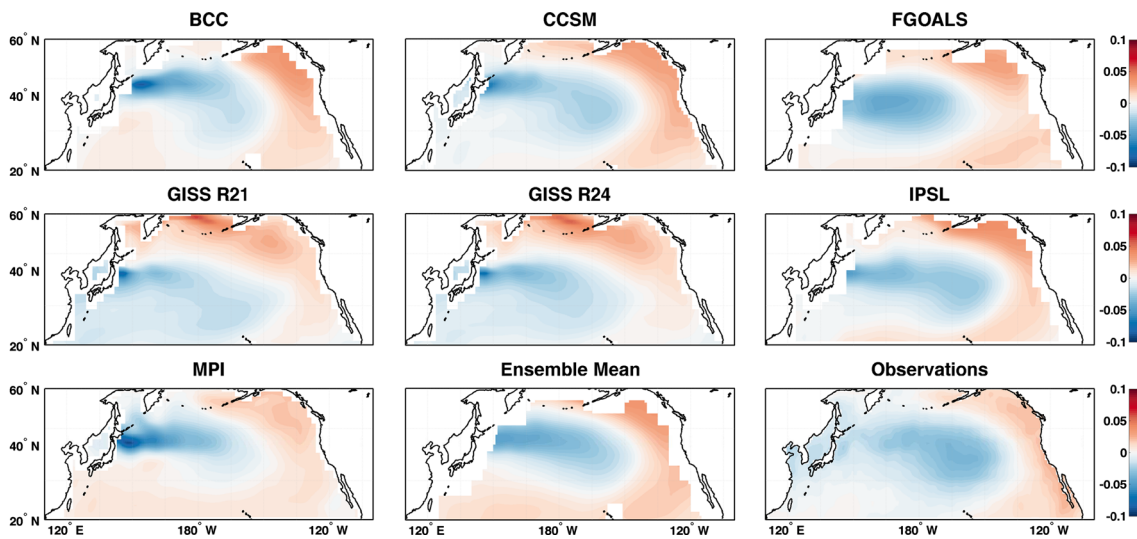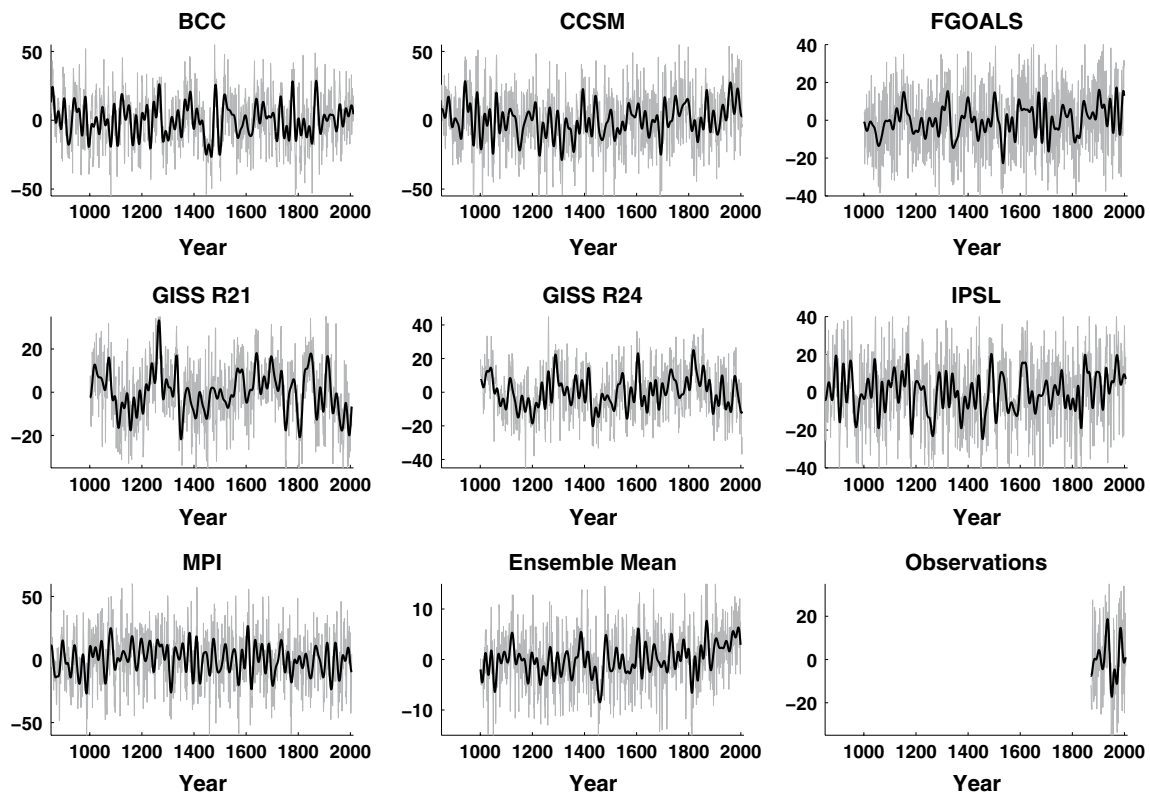
Fig. 2 Winter PDO loading pattern for simulations and observations (HadISST)

Fig. 3 The time series of the leading mode of the summer SST in the North Pacific Ocean domain is shown by the *grey line*. The time series of the 21-year low pass filtered leading mode is shown by the *black line*

The Ensemble Mean, BCC, and CCSM have decadal peak frequencies at ~10, ~20, and ~20 years, respectively. The peak frequency occurs at about 35 years for MPI. Peak frequency occurs at about 65 years for GISS R21, GISS

R24, and IPSL. Winter observations have significant broadband power in the PDO between 30 and 100 years. Similar to the summer PDO, correlations between the annual modeled and observed winter PDO index are low, largely

Fig. 4 The time series of the leading mode of the winter SST in the North Pacific Ocean domain is shown by the *grey line*. The time series of the 21-year low pass filtered leading mode is shown by the *black line*

non-significant, and vary in sign (Table 3; $r = -0.09$ to 0.24).

Figures 3 and 4 compare the low frequency (decadal and longer) variability in the individual modeled and observed 21-year low pass filtered for summer and winter, which shows no obvious temporal coherence. Correlations between all the low pass filtered series (Tables 4, 5) show no overall pattern of similarity, and correlations between the modeled PDO against observations vary in sign during their common period (summer, $r = -0.24$ to 0.40; winter, $r = -0.26$ to 0.26). The PDO time series for ERSST and HadISST show good agreement for both summer and winter ($r = 0.91$ and $r = 0.90$, respectively, $p \ll 0.01$). As the datasets agree on both the loadings and time series, we limited our further discussion to analyses using HadISST.

Results of the evolutive spectral analysis for the summer and winter PDO indices are shown in Figs. 7 and 8, respectively. All models show variable power in decadal to multidecadal wavelengths throughout the last millennium in both seasons. A number of the models, but in particular FGOALS as described above, also retain detectable interannual power in the leading mode of North Pacific SST variability. MPI shows strong variability in 20–30 year periods, which is most intense near ~1100, 1425, 1600, and 1950 in summer and winter. FGOALS, GISS R21, GISS R24, and IPSL display variable power in the 30–80 year period. For FGOALS, the highest intensity occurs near ~1300, 1500, and 1800 in summer and ~1350 and 1500 in winter. GISS R21 displays the most power near 1250 in summer and winter. GISS R24 displays the most power near 1400, 1600, and 1800 in summer, and 1200 and 1800 in winter. IPSL shows the most power near 1250 and 1475 in summer and winter. The Ensemble Mean shows strong variability in the 30–80 year period at ~1400 for both summer and winter. The shorter observational PDO indices provide limited opportunities to examine spectral variability through time; however, the increase in low frequency amplitude that can be seen in the observed PDO after the early twentieth century is also evident in the increase in multidecadal power in both seasons in Figs. 7 and 8.
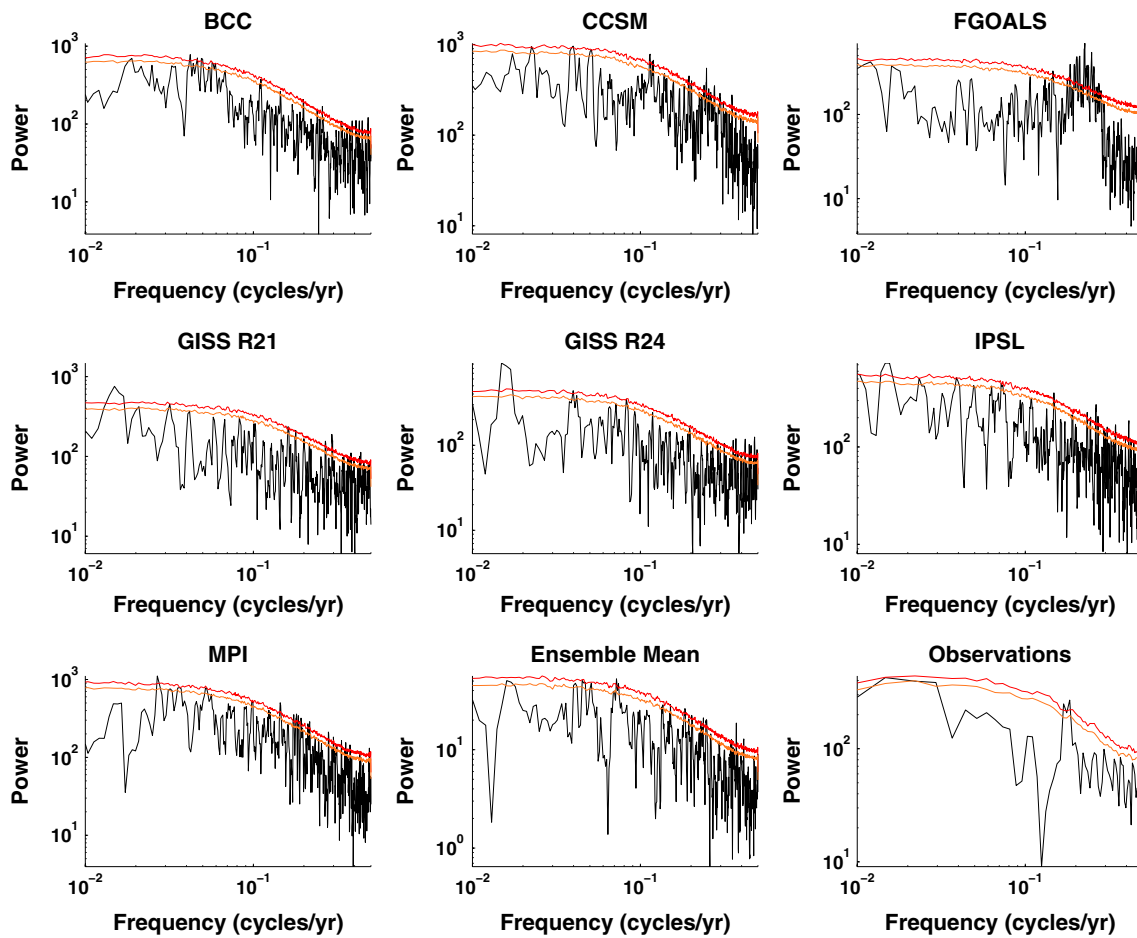
Fig. 5 Power spectrum of the summer PDO index is shown by the *black line*. The 90 and 95 % significance levels are shown by the *orange* and *red lines*, respectively

Table 2 Pearson product moment correlation coefficients between the summer PDO time series shown in Fig. 3, for the full period of overlap

	CCSM	FGOALS	GISS R21	GISS R24	IPSL	MPI	Ensemble	Observations
BCC	0.064	−0.025	0.021	0.041	−0.023	−0.007	0.382*	0.161
CCSM		−0.001	−0.027	−0.001	−0.035	−0.081*	0.416*	0.039
FGOALS			0.009	−0.012	0.008	−0.002	0.401*	−0.124
GISS R21				0.034	−0.032	0.024	0.226*	−0.077
GISS R24					0.013	0.076*	0.287*	−0.049
IPSL						0.028	0.369*	−0.195
MPI							0.357*	−0.041
Ensemble								−0.078

Correlations that are significant at $p < 0.05$ as determined using the method described by Ebisuzaki (1997) are marked by asterisks

3.2 Teleconnections

3.2.1 Precipitation

Field correlations between the summer (April–September) PDO index and the corresponding gridded precipitation data

are shown in Fig. 9. Observations reveal positive correlations between summer PDO and summer rainfall in the western United States, and negative correlation with rainfall in eastern China and tropical Asia, although these relationships are not significant at $p < 0.05$. For all models the summer PDO correlates positively with simulated precipitation over

Table 3 Pearson product moment correlation coefficients between the winter PDO time series shown in Fig. 4, for the full period of overlap

	CCSM	FGOALS	GISS R21	GISS R24	IPSL	MPI	Ensemble	Observations
BCC	0.083*	−0.014	0.045	0.012	0.024	0.022	0.467*	0.176
CCSM		0.003	−0.054	0.008	−0.018	−0.097*	0.390*	−0.007
FGOALS			−0.026	−0.009	0.041	0.001	0.342*	−0.092
GISS R21				0.102	−0.100*	0.037	0.103*	0.237*
GISS R24					−0.039	0.043	0.157*	0.075
IPSL						0.009	0.361*	−0.063
MPI							0.395*	−0.091
Ensemble								0.068

Correlations that are significant at $p < 0.05$ as determined using the method described by Ebisuzaki (1997) are marked by asterisks
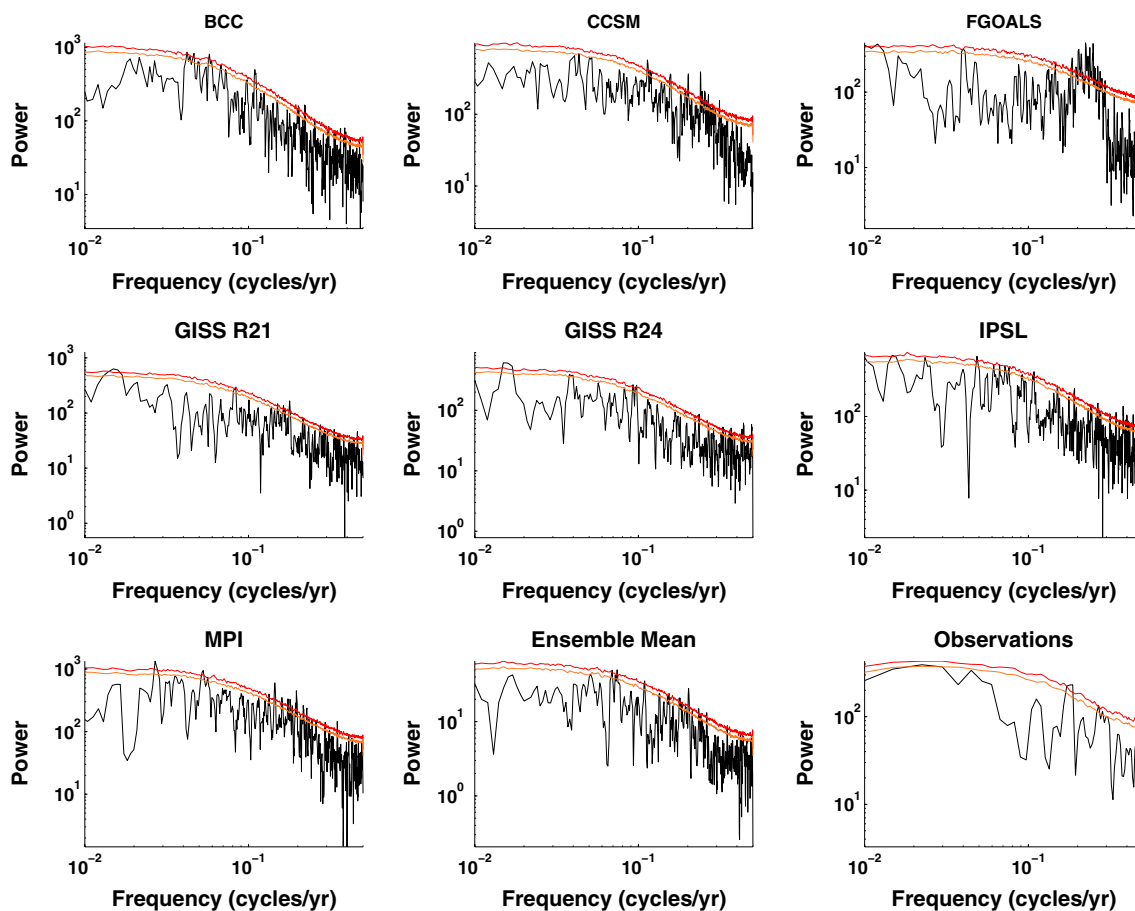
Fig. 6 Power spectrum of the winter PDO index is shown by the *black line*. The 90 and 95 % significance levels are shown by the *orange* and *red lines*, respectively

the west coast of the United States. BCC, CCSM, FGOALS, IPSL, and MPI match the negative correlation in eastern Russia and Alaska.

Figure 10 shows the correlations fields between the winter (October–March) PDO index and the corresponding modeled precipitation data. For the observed winter PDO and precipitation there are significant positive correlations over

Mexico and the central and southwestern United States, and significant negative correlations over the Pacific Northwest of the United States and western Canada. Significant negative correlations are also observed over eastern Russia and northeastern South America. FGOALS, GISS R21, IPSL, MPI, and the Ensemble Mean show positive correlations in the southern United States and negative correlations in the

Table 4 Pearson product moment correlation coefficients between the 21-year summer low pass filtered time series shown in Fig. 3, for the full period of overlap

	CCSM	FGOALS	GISS R21	GISS R24	IPSL	MPI	Ensemble	Observations
BCC	0.058	−0.014	0.071	0.049	−0.048	0.010	0.464*	−0.089
CCSM		−0.003	−0.138	0.045	0.025	−0.121*	0.436*	0.214
FGOALS			0.007	−0.088	−0.019	−0.002	0.322*	−0.243
GISS R21				0.080	−0.162	0.060	0.123*	−0.134
GISS R24					0.168	0.068*	0.346*	0.106
IPSL						0.039	0.373*	−0.067
MPI							0.324*	0.396
Ensemble								0.116

Correlations that are significant at $p < 0.05$ as determined using the method described by Ebisuzaki (1997) are marked by asterisks

Table 5 Pearson product moment correlation coefficients between the 21-year winter low pass filtered PDO time series shown in Fig. 4, for the full period of overlap

	CCSM	FGOALS	GISS R21	GISS R24	IPSL	MPI	Ensemble	Observations
BCC	0.144*	0.025	0.068	0.009	0.034	0.074	0.570*	0.094
CCSM		0.030	−0.202	0.009	0.084	−0.187*	0.438*	−0.012
FGOALS			−0.010	−0.128	0.149	−0.067	0.378*	−0.258
GISS R21				0.178	−0.249*	0.041	−0.049*	0.013*
GISS R24					0.109	0.031	0.125*	0.258
IPSL						−0.005	0.453*	0.033
MPI							0.277*	−0.032
Ensemble								0.042

Correlations that are significant at $p < 0.05$ as determined using the method described by Ebisuzaki (1997) are marked by asterisks

Pacific Northwest. Only CCSM has negative correlations in Alaska. BCC, FGOALS, IPSL, MPI, and the Ensemble Mean show negative correlations in eastern Russia. All models show a positive correlation in the northeastern parts of the Pacific, and a negative correlation in the southwestern parts of the Pacific.

Correlations between the modeled October–March PDO index and the following corresponding summer (April–September) precipitation data are shown in Fig. 11. Observations suggest similar correlation patterns to those for the coeval summer, with positive correlations between winter PDO and summer precipitation in western North America and negative correlations in tropical Asia, but these are not significant at $p < 0.05$. BCC, CCSM, FGOALS, and GISS R21 have positive correlations on the west coast of the United States. FGOALS also has negative correlations in eastern Asia. The summer, winter, and lagged precipitation field correlations are all globally significant. Teleconnection patterns for the historical simulations only are highly similar to those reported above and available in Supplemental Material.

3.2.2 Sea level pressure

Figures 12 and 13 show the correlations field between the summer and winter PDO index and the corresponding seasonal sea level pressure data, respectively. For summer observations, the PDO correlated negatively in the contiguous United States and in eastern Asia, but positively in eastern Russia and Alaska. CCSM, GISS R21, GISS R24 and IPSL, and the Ensemble Mean agreed with observations in these areas. FGOALS and MPI showed negative correlations in Asia and positive correlations in Russia and Alaska, but also showed positive correlations in the contiguous United States. BCC and the Ensemble Mean showed positive correlations in Russia and Alaska, and negative correlations in eastern Asia, but did not have significant correlations in the contiguous United States.

In winter, the PDO correlates negatively in Asia, Russia, and Alaska, and positively in the contiguous United States. MPI, and the Ensemble Mean agree with observations for Russia, Alaska, and the contiguous United States, but either show positive correlations or do not have significant correlations in Asia. CCSM, FGOALS, and IPSL agree with observations in Russia and Alaska, but not in Asia or the contiguous United States. BCC agrees with observations in the United States but not in Asia. GISS R21 and GISS R24 do not agree with observations in any of those locations. The sea level pressure field correlations for all models and observations are globally significant for summer and winter. Teleconnection patterns for the historical simulations only are
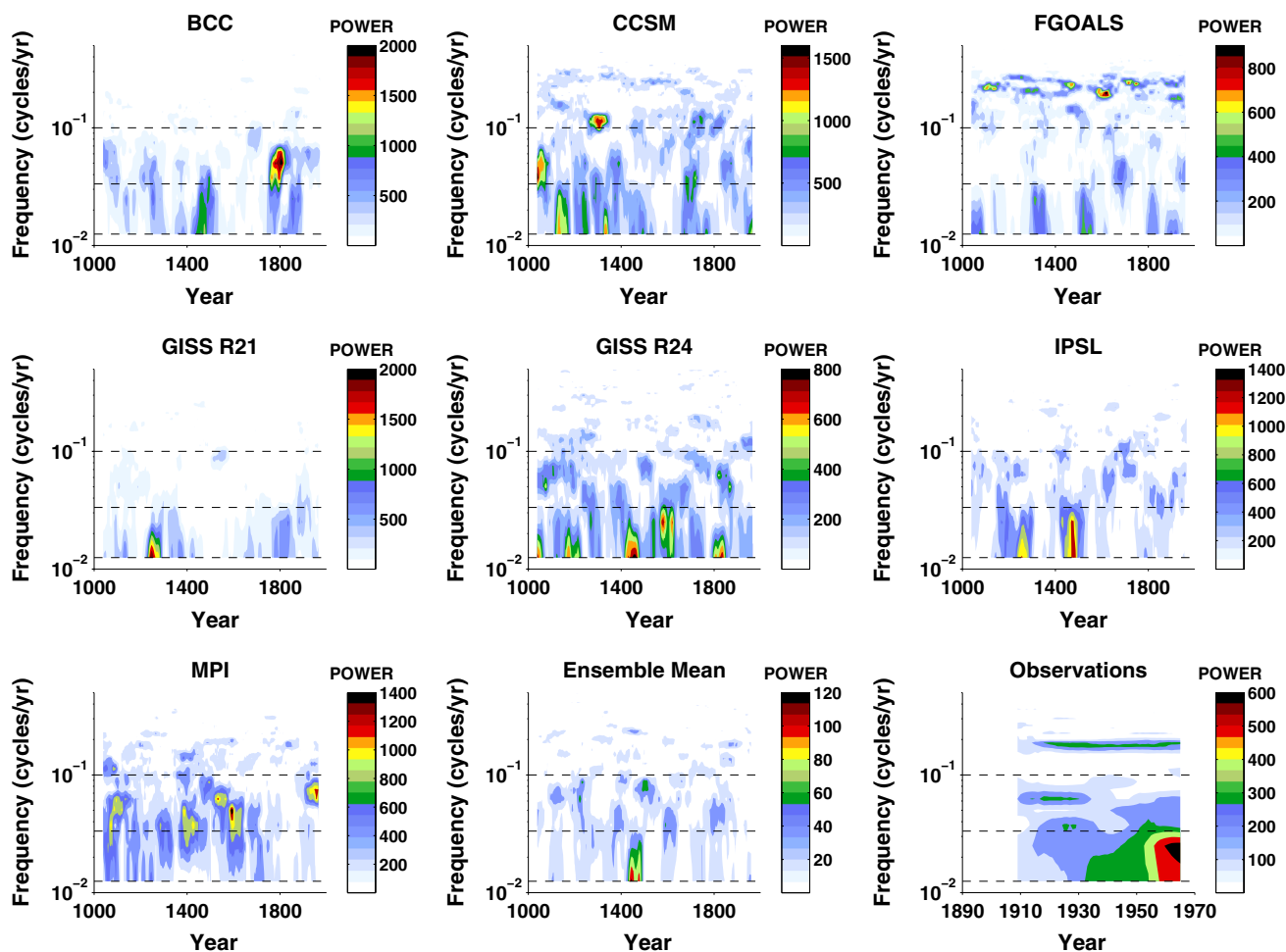
Fig. 7 Evolutive power spectrum based on performing the summer MTM analysis with a moving 80-year window. *Dashed black horizontal lines* in each plot indicate, from the *top*, the 10-year, 30-year, and 80-year periodicity

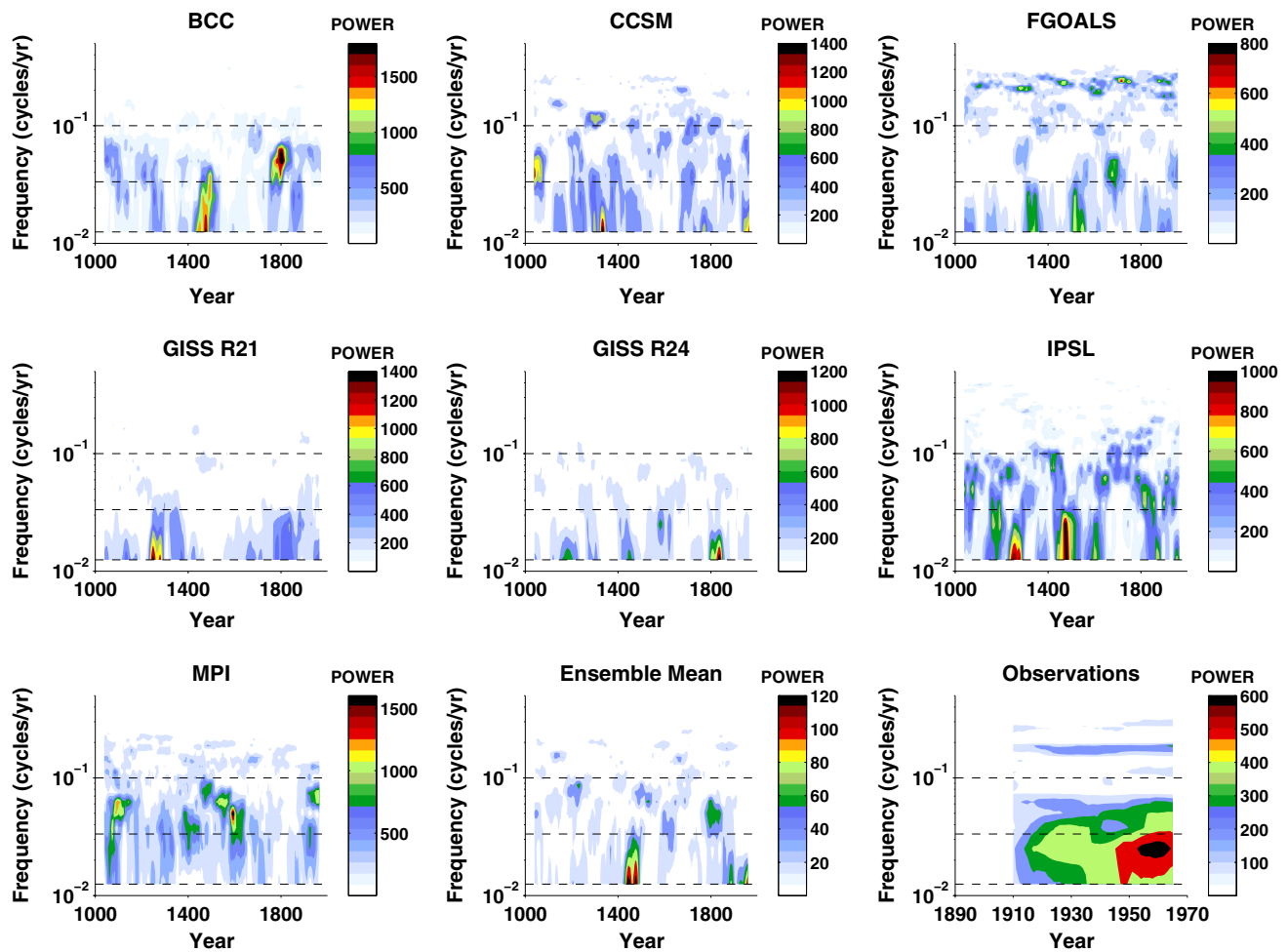highly similar to those reported above and available in Supplemental Material.

3.2.3 Surface temperature

The correlations between surface air temperature data and the April–September PDO index are shown in Fig. 14. PDO in observations correlates positively with temperatures in eastern Russia, Alaska, off the west coast of the United States, and in the tropical Pacific. They also show negative correlations over Japan and the central North Pacific. All models agree with observations in these locations. The observations correlate positively in the tropical Pacific Ocean. All models except GISS R21 and GISS R24 agree with observations in the tropical Pacific.

Figure 15 shows the correlations between the October–March PDO index and surface temperatures. Observations correlate negatively with GISTEMP in the central North Pacific and positively in the Bering Sea, Alaska, and off the

west coast of the United States. All models agree with observations in these areas. Observations correlate negatively in northern Asia and positively in southern Asia. BCC, CCSM, FGOALS, IPSL, and MPI agree with observations in Asia. GISS R21 and GISS R24 correlate negatively throughout Asia.

Correlations between the October–March PDO index and subsequent the April–September surface temperature data are shown in Fig. 16. The observations are negatively correlated with summer temperatures for the central North Pacific and positively in the Gulf of Alaska, off the west coast of the United States, and toward the tropical Pacific Ocean. BCC, CCSM, FGOALS, IPSL, MPI, and the Ensemble Mean agree with observations in these areas. GISS R21 and GISS R24 correlate negatively everywhere in the Northern Hemisphere except the Gulf of Alaska and off the west coast of the United States. The summer, winter, and lagged surface temperature field correlations are all globally significant. Teleconnection patterns for the historical simulations only

Fig. 8 Evolutive power spectrum based on performing the winter MTM analysis with a moving 80-year window. *Dashed black horizontal lines in each plot indicate, from the top, the 10-, 30-, and 80-year periodicity*

are highly similar to those reported above and available in Supplemental Material.

4 Discussion

All models produce a multidecadal mode of North Pacific variability over the last millennium with spatial and spectral patterns similar to observations. This finding is consistent with other assessment of transient historical (c.f. Stoner et al. 2009; Deser et al. 2012; Polade et al. 2013; Sheffield et al. 2013; Yim et al. 2015) and long control simulations (c.f. Hunt 2008). As would be expected of a climate mode that reflects predominantly internal climate system variability, no model examined here reproduces the precise observed secular time history of the PDO over the last century and all models have different time histories. This suggests that North Pacific decadal variability, as simulated by the models and defined by the PDO index, does not reflect a consistent

dynamic response to radiative forcing over this time period, but rather is dominated by internal climate system variation. Indeed, Schneider and Cornuelle (2005) have shown that the observed PDO can be explained as the superposition of interannual- and decadal-scale ocean–atmosphere variability in the El Niño-Southern Oscillation (ENSO), Aleutian Low, and Kuroshio-Oyashio Extension (KOE). Newman et al. (2003) demonstrated that the PDO could be modeled as a function of ENSO and atmospheric noise. These studies suggest that the PDO is not an independent dynamical feature of the climate system, but rather is dependent on ENSO and reflects internal ocean–atmosphere variability. While ENSO is thought to potentially respond to past radiative forcing changes based on model simulations (e.g. Clement et al. 1996; Ault et al. 2013), paleoclimate reconstructions do not demonstrate such an influence over the last millennium, at least at decadal to multidecadal time scales (Ault et al. 2013; Emile-Geay et al. 2013; Tierney et al. 2015), and modeling studies further suggest that only substantial
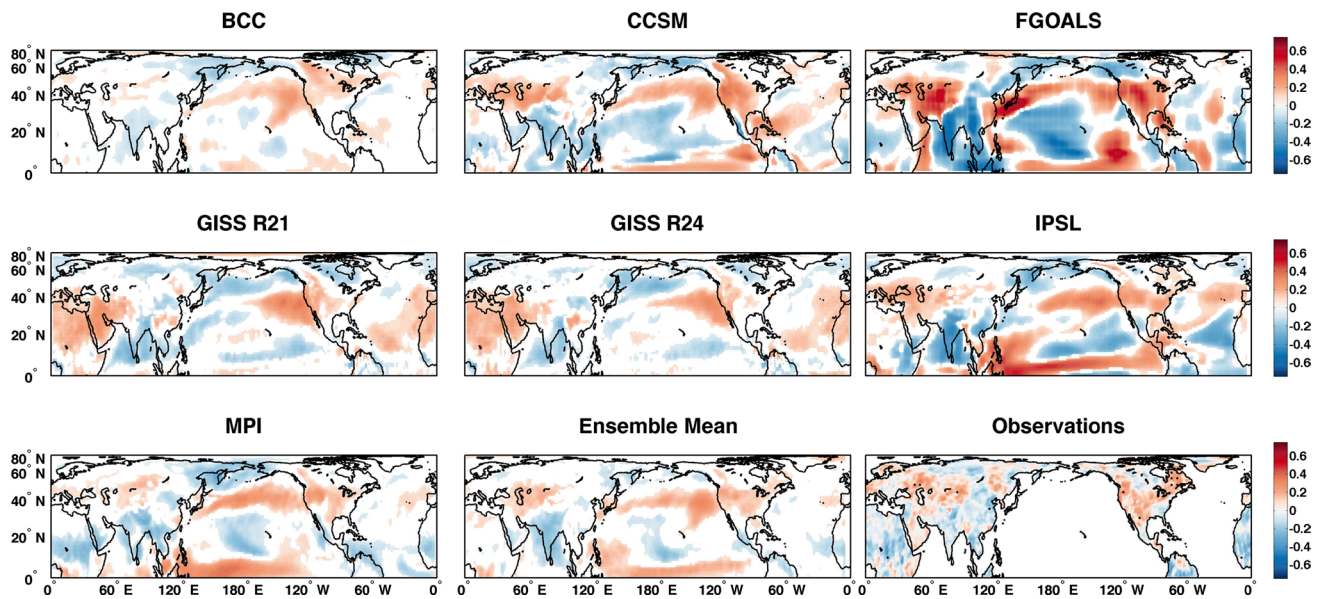
Fig. 9 Field correlation between the summer PDO index and summer precipitation. For the models, only correlations that are significant at $p < 0.05$ are shown. For observations, the *black dots* represent regions where the correlation is significant at $p < 0.05$. GPCC precipitation observations are from Schneider et al. (2011)
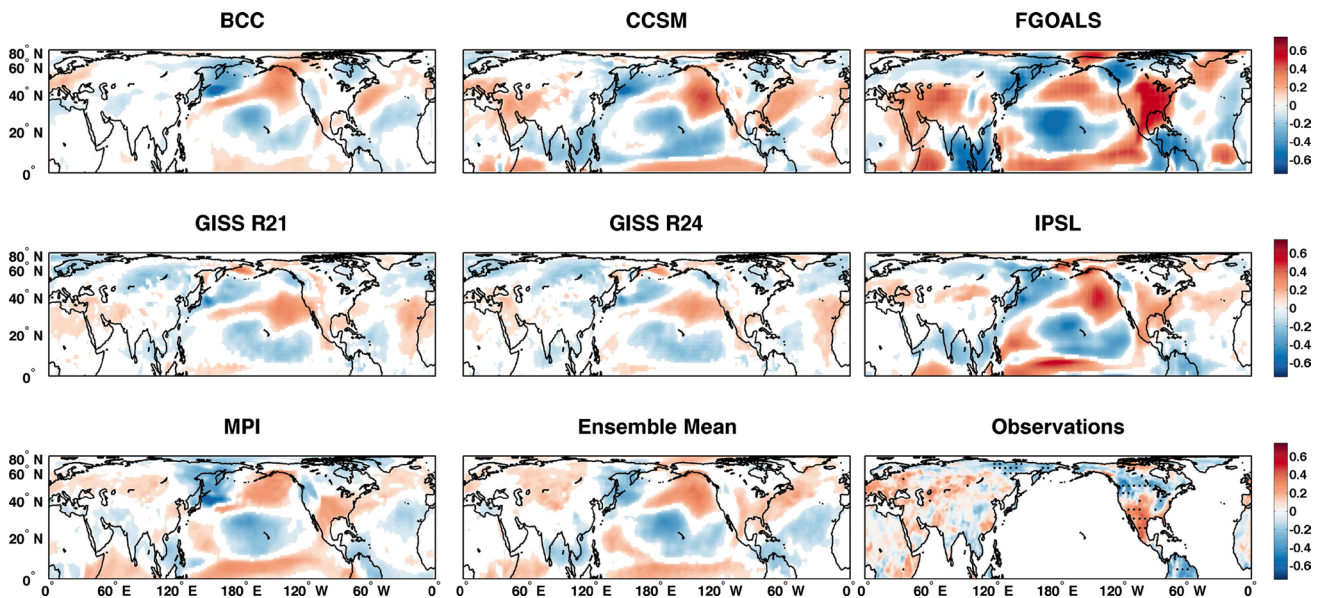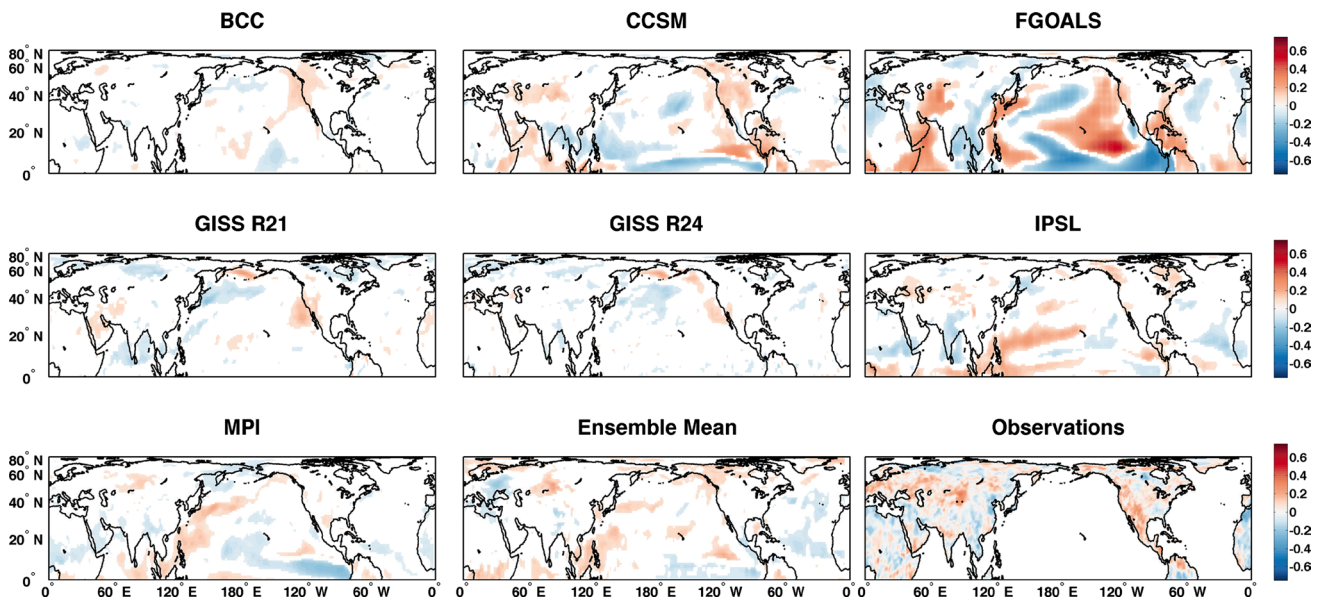

Fig. 10 Field correlation between the winter PDO index and winter precipitation. For the models, only correlations that are significant at $p < 0.05$ are shown. For observations (GPCC), the *black dots* represent regions where the correlation is significant at $p < 0.05$. GPCC precipitation observations are from Schneider et al. (2011)

changes to insolation may result in a detectable forced alteration of ENSO variance (e.g. Emile-Geay et al. 2008; Phipps et al. 2013). Further analysis of the full Pacific Ocean domain indicates that observed Pacific decadal variability is not restricted to the Northern Hemisphere (Garreaud and Battisti 1999), further suggesting a common tropical driver of the phenomena (Evans et al. 2001a; Newman et al. 2003).

Our observation here that the modeled PDO does not have a strong or consistent response to forcing in the past1000 simulations agrees with Landrum et al. (2013b), who came to the same conclusion for the last millennium simulation in the CCSM4 model.

We note in some models the EOF patterns indicate stronger loadings than calculated from observations (Figs. 1, 2). While

Fig. 11 Field correlation between the winter PDO index and the following summer precipitation. For the models, only correlations that are significant at $p < 0.05$ are shown. For observations, the *black dots* represent regions where the correlation is significant at $p < 0.05$. GPCC precipitation observations are from Schneider et al. (2011)
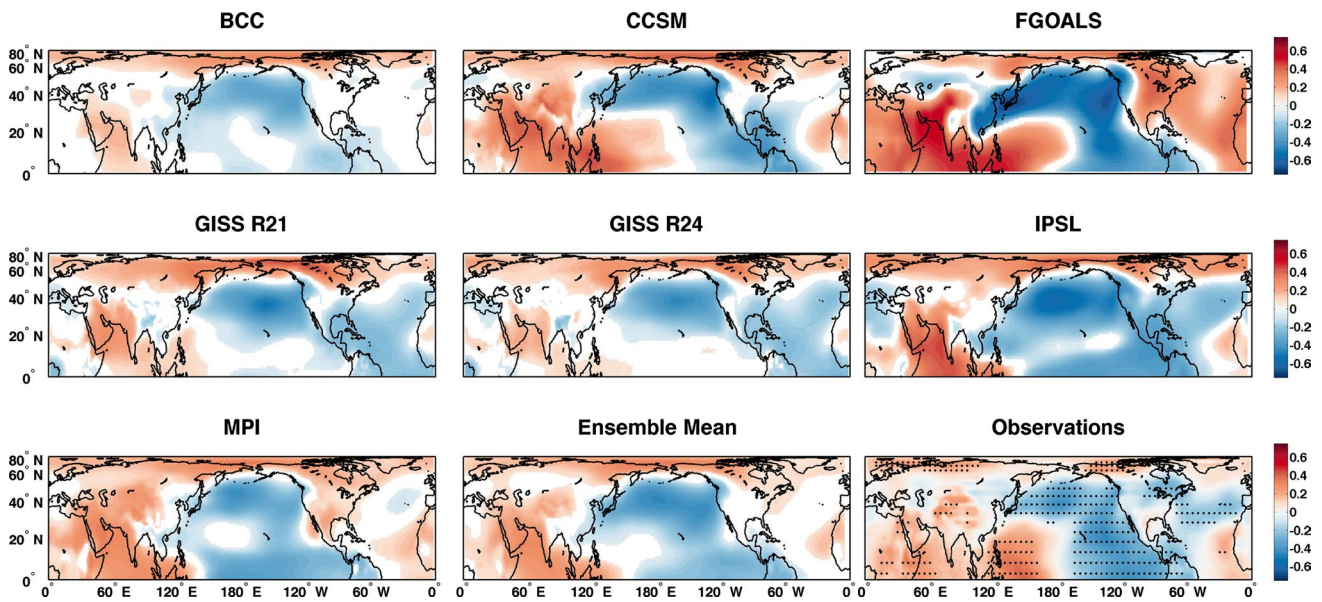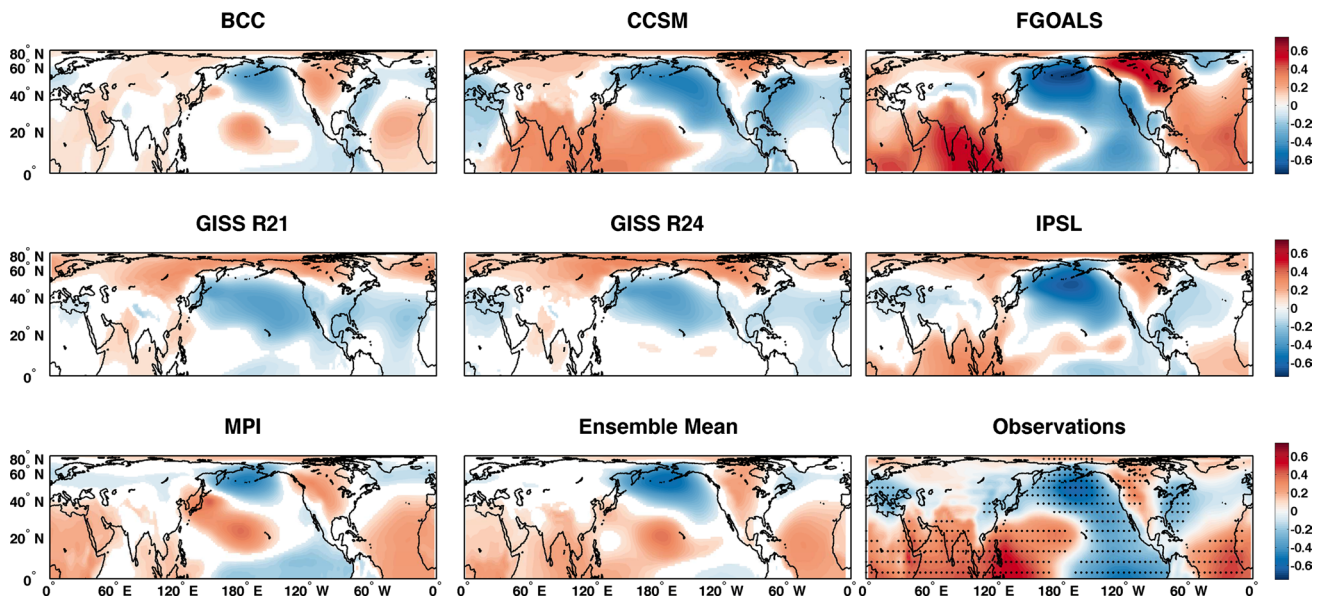

Fig. 12 Field correlation between the summer PDO index and summer sea level pressure. For the models, only correlations that are significant at $p < 0.05$ are shown. For observations, the *black dots* represent regions where the correlation is significant at $p < 0.05$. Observations for sea level pressure are from Compo and Sardeshmukh (2006)

caution is necessary when interpreting the magnitude of these loading values when models and observations differ from one another in total length and spatial resolution, this suggests that PDO mode variance in some models may be larger and more coherent than in observations. One implication of this could be that teleconnections to regional climate are stronger and more coherent in these models compared to the real world,

a possibility that needs to be kept in mind when comparing proxy reconstructions and forced paleoclimate model simulations of the last millennium.

There is no obvious or linear association with estimated solar variability over the last millennium in the majority of the models (Schmidt et al. 2011). While the PDO in MPI does have significant spectral power near the ~11-year solar

Fig. 13 Field correlation between the winter PDO index and winter sea level pressure. For the models, only correlations that are significant at $p < 0.05$ are shown. For observations, the *black dots* represent regions where the correlation is significant at $p < 0.05$. Observations for sea level pressure are from Compo and Sardeshmukh (2006)
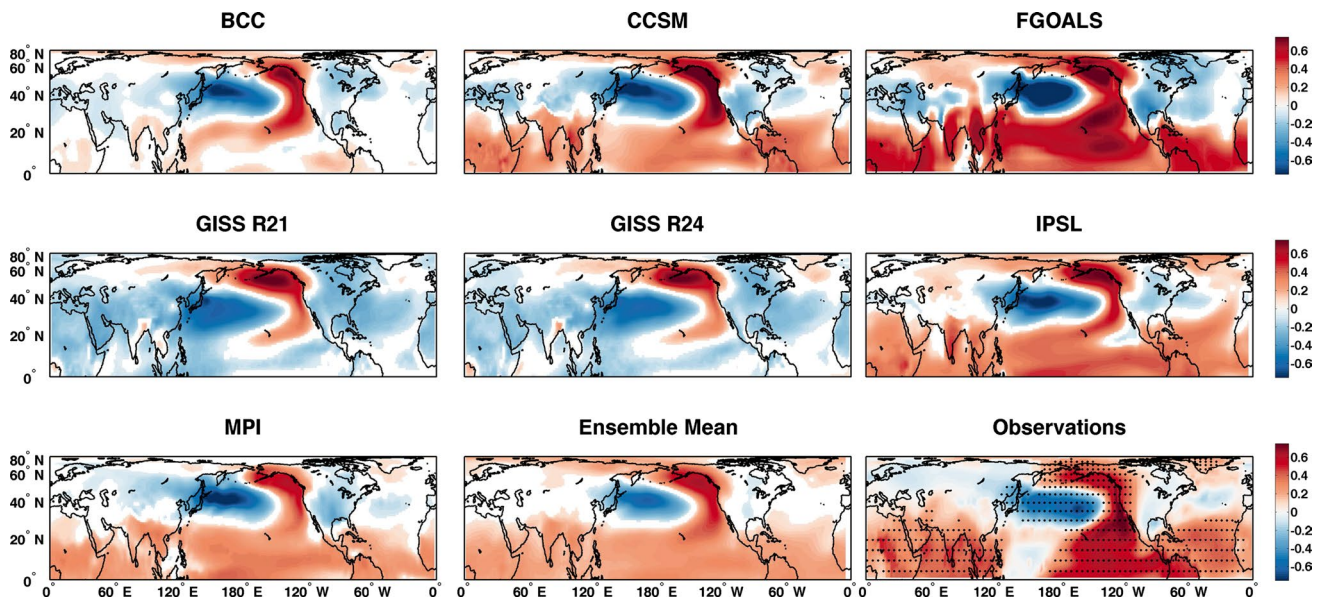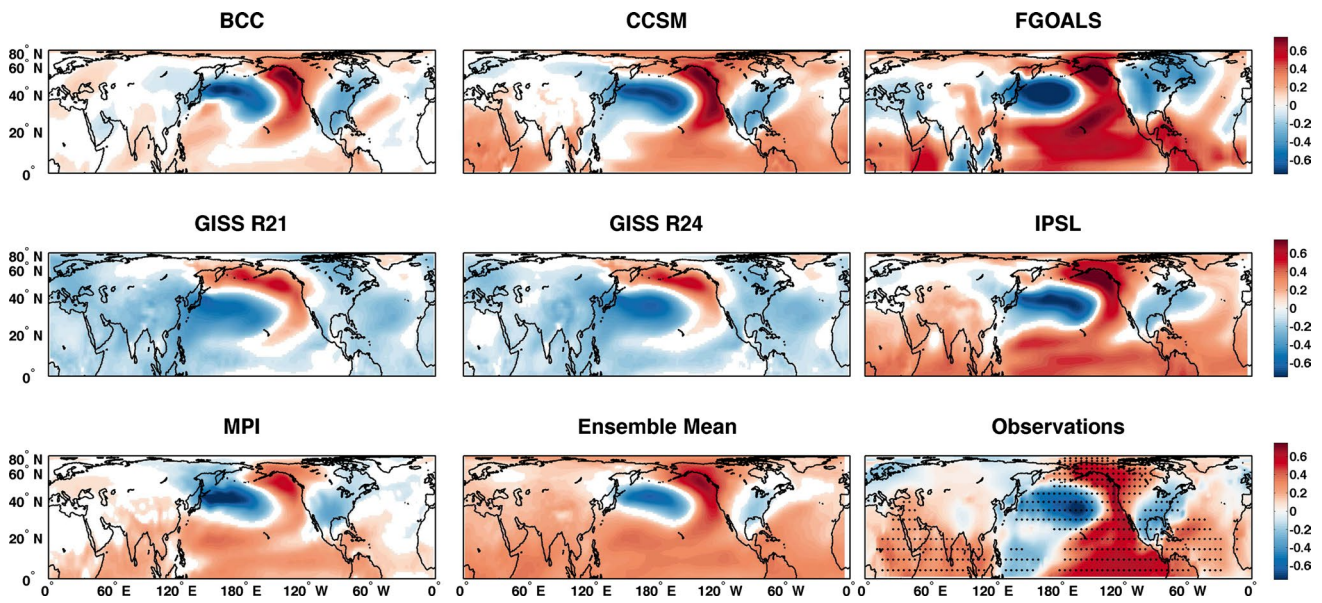

Fig. 14 Field correlation between the summer PDO index and summer near-surface air temperature. For the models, only correlations that are significant at $p < 0.05$ are shown. For observations, the *black dots* represent regions where the correlation is significant at $p < 0.05$. Observations for surface temperature are from Hansen et al. (2010)

cycle in both seasons, we find that it has no relationship with either the amplitude or phase of the corresponding solar forcing applied to the model. Nor does there appear to be a coherent responses to changes in volcanic forcing. Modeled PDO does not behave consistently following major volcanic eruptions in the later thirteenth century (Lavigne et al. 2013), 1450s (Gao et al. 2006), or early nineteenth century (Figs. 3,

4). For instance, although one of the GISS ensemble members (R21) simulated a negative phase of the PDO coincident with the timing of late thirteenth century eruptions (Schmidt et al. 2012), the same ensemble member simulates a positive phase after early nineteenth century eruptions. Likewise, BCC has a negative phase PDO in the late thirteenth century, but a positive phase in the 1450s. There is no consistency in

Fig. 15 Field correlation between the winter PDO index and winter near-surface air temperature. For the models, only correlations that are significant at $p < 0.05$ are shown. For observations, the *black dots* represent regions where the correlation is significant at $p < 0.05$. Observations for surface temperature are from Hansen et al. (2010)
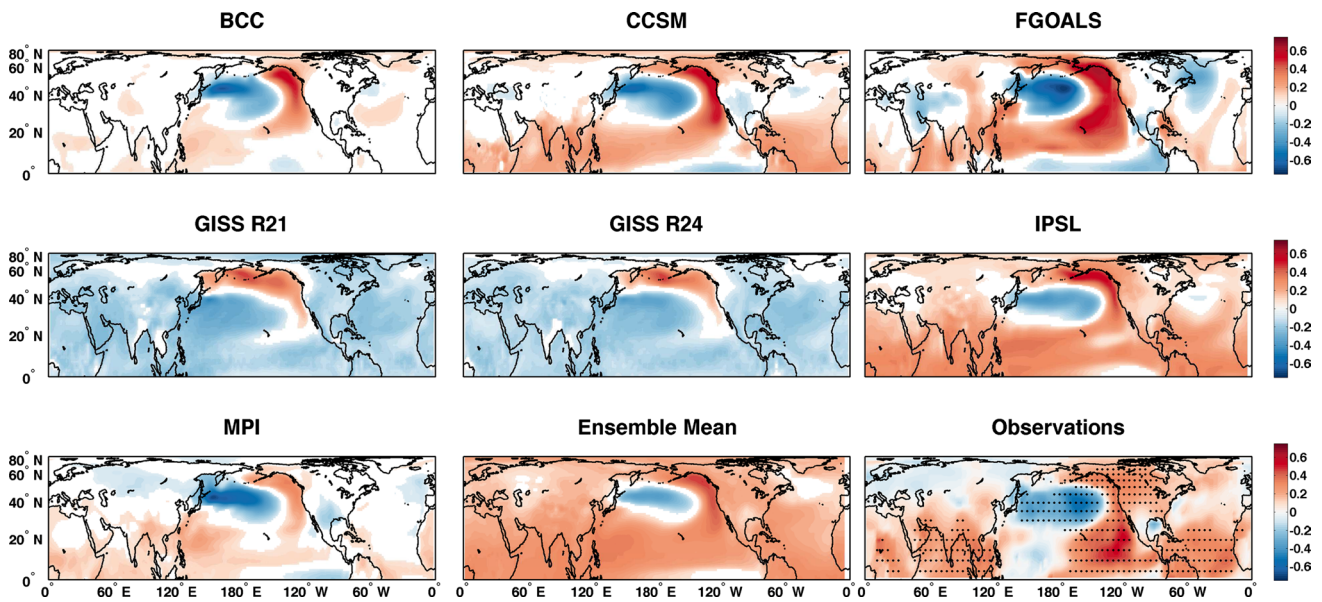
Fig. 16 Field correlation between the winter PDO index and following summer near-surface air temperature. For the models, only correlations that are significant at $p < 0.05$ are shown. For observations, the *black dots* represent regions where the correlation is significant at $p < 0.05$. Observations for surface temperature are from Hansen et al. (2010)

the behavior after eruptions within each model. We conclude that, from the point of view of the forced model simulated ensemble response, there is no evidence for a consistent influence from changes in volcanic and solar forcing on the PDO. Our observations are consistent with the findings by Zanchettin et al. (2012), who examined decadal variability

in the MPI, and Landrum et al. (2013b) who examined the PDO in a last millennium simulation using the CCSM4. This is not necessarily an unexpected finding, since by definition the global mean temperature signal is removed when calculating the PDO index. However, this does suggests that, at least in the GCMs considered here, either external forcing

does not consistently excite particular modes of decadal scale variability in the North Pacific or the signal is smaller than the internal variability of the system.

Our evaluation of spatial patterns, spectral power density, and teleconnection fidelity suggest that overall CCSM, FGOALS, and IPSL are the most similar to observations in the aggregate. These models reproduce the spatial pattern of the observed PDO for both summer and winter. The observed summer (winter) power spectrum of the observations has broadband maximum power in the range of 30–65 (30–100) years, which these models largely reproduce, although FGOALS has considerable interannual power as well. BCC also has a similar spatial pattern to the observed summer PDO and has multidecadal power in both seasons similar to the observations, but performs less well with respect to the winter spatial pattern. GISS and MPI likewise have similar spatial patterns but lack statistically significant multidecadal spectral power in the range of the observations. The Ensemble Mean reproduces the spatial patterns and had statistically significant multidecadal spectral pattern that matches observations.

Lacking high resolution extra-tropical marine proxy records, most paleoclimate reconstructions of North Pacific decadal variability rely on distal terrestrial or tropical marine proxies. The proxy paleoclimate reconstructions of D'Arrigo et al. (2001), Evans et al. (2001b), Biondi et al. (2001), Gedalof and Smith (2001), and D'Arrigo and Wilson (2006), for example, use tree-ring sites in the southwestern United States, the Gulf of Alaska, Mongolia, Japan, China, and eastern Russia (see Supplemental Material). These records are sensitive to local temperature (Gulf of Alaska, Russia) or soil moisture (southwestern North America, central and monsoon Asia), and PDO reconstructions that rely on these assume a stable teleconnection between variability in the North Pacific and their terrestrial climate. While we don't expect that model simulated PDO will have the same secular temporal history as the actual PDO, understanding the fidelity of model teleconnections to terrestrial climate is useful for several reasons. First, the models do allow for assessments of the possible sources of disagreement between reconstruction, including nonstationary teleconnections (Gershunov and Barnett 1998; McCabe et al. 2004a; McAfee 2014; Wise 2014) and proxy network selection, within a pseudoproxy framework (Smerdon 2011). Second, establishing which models have reasonable overall teleconnections provides can guide their use for paleoclimate data assimilation (c.f. Steiger et al. 2014).

Of the models considered here, BCC, CCSM, FGOALS, IPSL, and the Ensemble Mean best reproduce the observed teleconnections in the regions used for the reconstructions in southwestern United States, Alaska, Russia, and eastern Asia (Figs. 9, 10, 11, 12, 13, 14, 15, 16). Although statistically

significant correlations between summer PDO and summer precipitation can be sparse within these models, particularly in Asia, they generally agree in sign with observations. These models agree with observations in the southwestern United States, Alaska, Russia, and parts of Asia for the correlation between summer (winter) PDO and surface temperature, but disagree across China (Mongolia and eastern Russia). MPI agrees moderately well with observed teleconnections. The GISS model simulations show the least similar patterns compared to observed teleconnections for those regions with proxy data used to reconstruct the PDO. Taking into account the spatial and spectral fidelity discussed earlier, CCSM, FGOALS, and IPSL appear likely to be the most appropriate models to use in PDO pseudoproxy analyses and other paleoclimate model/data comparisons.

5 Summary and conclusions

We have evaluated the spatiotemporal and spectral properties of the Pacific decadal oscillation as simulated by model experiments of the past1000 years. All the models produce spatial loading patterns similar to the observed PDO, and most produce a leading mode of North Pacific temperature variability with significant decadal and multidecadal power. There is no indication, either within individual simulations nor across the ensemble, of a coherent forced response, suggesting the PDO as defined here and as simulated in the models reflects predominantly internal climate system variability. Interestingly, all the models considered here show temporal changes in the power associated with decadal-scale variability (Figs. 7, 8), which suggests the magnitude of the influence of the PDO on Pacific Ocean basin climate may indeed wax and wane through time. This review of the characteristics of North Pacific decadal variability in the last millennium (past1000) CMIP5 simulations and of the ability of this current generation of long forced GCM simulations to reproduce climate features of the observed ocean–atmosphere system now allows us to now apply these simulations toward evaluating how this variability may be imprinted on terrestrial or distal marine proxies of the last millennium.

References

Ault TR, Deser C, Newman M, Emile-Geay J (2013) Characterizing decadal to centennial variability in the equatorial pacific during the last millennium. Geophys Res Lett 40(13):3450–3456. doi:10.1002/grl.50647

Biondi F, Gershunov A, Cayan DR (2001) North Pacific decadal climate variability since 1661. J Clim 14:5–10

Bothe O, Jungclaus JH, Zanchettin D (2013) Consistency of the multi-model CMIP5/PMIP3-past1000 ensemble. Clim Past 9(6):2471–2487. doi:10.5194/cp-9-2471-2013

Brown PT, Li W, Li L, Ming Y (2014) Top-of-atmosphere radiative contribution to unforced decadal global temperature variability in climate models. Geophys Res Lett 41(14):5175–5183. doi:10.1002/2014gl060625

Buckley B, Anchukaitis K, Penny D, Fletcher R, Cook E, Sano M, Nam L, Wichienkeeo A, Minh T, Hong T (2010) Climate as a contributing factor in the demise of Angkor, Cambodia. Proc Nat Acad Sci 107(15):6748–6752

Clement AC, Seager R, Cane MA, Zebiak SE (1996) An ocean dynamical thermostat. J Clim 9(9):2190–2196

Compo GP, Whitaker JS, Sardeshmukh PD, Matsui N, Allan R, Yin X, Gleason B, Vose R, Rutledge G, Bessemoulin P et al (2011) The twentieth century reanalysis project. Q J R Meteorol Soc 137(654):1–28

Compo JWGP, Sardeshmukh P (2006) Feasibility of a 100 year reanalysis using only surface pressure data. Bull Am Meteorol Soc 87:175–190

Crowley TJ (2000) Causes of climate change over the past 1000 years. Science 289:270–277

Crowley TJ, Zielinski G, Vinther B, Udisti R, Kreutz K, Cole-Dai J, Castellano E (2008) Volcanism and the little ice age. PAGES News 16(2):22–23

D'Arrigo R, Wilson R (2006) On the Asian expression of the PDO. Int J Climatol 26(12):1607–1617

D'Arrigo R, Villalba R, Wiles G (2001) Tree-ring estimates of Pacific decadal climate variability. Clim Dyn 18:219–224

Deser C, Phillips AS, Alexander MA (2010) Twentieth century tropical sea surface temperature trends revisited. Geophys Res Lett. doi:10.1029/2010GL043321

Deser C, Phillips AS, Tomas RA, Okumura YM, Alexander MA, Capotondi A, Scott JD, Kwon YO, Ohba M (2012) ENSO and pacific decadal variability in the community climate system model version 4. J Clim 25(8):2622–2651. doi:10.1175/jcli-d-11-00301.1

Deser C, Phillips AS, Alexander MA, Smoliak BV (2014) Projecting North American climate over the next 50 years: uncertainty due to internal variability. J Clim 27(6):2271–2296

Dufresne JL, Foujols MA, Denvil S, Caubel A, Marti O, Aumont O, Balkanski Y, Bekki S, Bellenger H, Benshila R, Bony S, Bopp L, Braconnot P, Brockmann P, Cadule P, Cheruy F, Codron F, Cozic A, Cugnet D, Noblet N, Duvel JP, Ethé C, Fairhead L, Fichefet T, Flavoni S, Friedlingstein P, Grandpeix JY, Guez L, Guilyardi E, Hauglustaine D, Hourdin F, Idelkadi A, Ghattas J, Joussaume S, Kageyama M, Krinner G, Labetoulle S, Lahellec A, Lefebvre MP, Lefevre F, Levy C, Li ZX, Lloyd J, Lott F, Madec G, Mancip M, Marchand M, Masson S, Meurdesoif Y, Mignot J, Musat I, Parouty S, Polcher J, Rio C, Schulz M, Swingedouw D, Szopa S, Talandier C, Terray P, Viovy N, Vuichard N (2013) Climate change projections using the IPSL-CM5 Earth System Model: from CMIP3 to CMIP5. Clim Dyn 40(9–10):2123–2165. doi:10.1007/s00382-012-1636-1

Ebisuzaki W (1997) A method to estimate the statistical significance of a correlation when the data are serially correlated. J Clim 10(9):2147–2153

Emile-Geay J, Seager R, Cane MA, Cook ER, Haug GH (2008) Volcanoes and enso over the past millennium. J Clim 21(13):3134–3148

Emile-Geay J, Cobb KM, Mann ME, Wittenberg AT (2013) Estimating central equatorial Pacific SST variability over the past millennium. Part II: Reconstructions and implications. J Clim 26(7):2329–2352

Evans MN, Cane MA, Schrag DP, Kaplan A, Linsley BK, Villalba R, Wellington GM (2001a) Support for tropically-driven Pacific decadal variability based on paleoproxy evidence. Geophys Res Lett 28:3689–3692

Evans MN, Kaplan A, Cane MA, Villalba R (2001b) Globality and optimality in climate field reconstructions from proxy data. In: Markgraf V (ed) Interhemispheric climate linkages. Cambridge University Press, Cambridge, pp 53–72

Evans MN, Kaplan A, Cane MA (2002) Pacific sea surface temperature field reconstruction from coral δ^{18}O data using reduced space objective analysis. Paleoceanography. doi:10.1029/2000PA000590

Gao C, Robock A, Ammann CM (2008) Volcanic forcing of climate over the past 1500 years: an improved ice-core-based index for climate models. J Geophys Res 113:D23111

Gao CC, Robock A, Self S, Witter JB, Steffenson JP, Clausen HB, Siggaard-Andersen ML, Johnsen S, Mayewski PA, Ammann C (2006) The 1452 or 1453 AD Kuwae eruption signal derived from multiple ice core records: greatest volcanic sulfate event of the past 700 years. J Geophys Res Atmos 111:D12107

Garreaud RD, Battisti DS (1999) Interannual (ENSO) and interdecadal (ENSO-like) variability in the Southern Hemisphere tropospheric circulation. J Clim 12:2113–2123

Gedalof Z, Smith DJ (2001) Interdecadal climate variability and regime-scale shifts in Pacific North America. Geophys Res Lett 28:1515–1518. doi:10.1029/2000GL011779

Gedalof Z, Mantua NJ, Peterson DL (2002) A multi-century perspective of variability in the Pacific decadal oscillation: new insights from tree rings and coral. Geophys Res Lett. doi:10.1029/2002GL015824

Gershunov A, Barnett TP (1998) Interdecadal modulation of ENSO teleconnections. Bull Am Meteorol Soc 79(12):2715–2725

Giorgetta MA, Jungclaus J, Reick CH, Legutke S, Bader J, Böttinger M, Brovkin V, Crueger T, Esch M, Fieg K, Glushak K, Gayler V, Haak H, Hollweg HD, Ilyina T, Kinne S, Kornblueh L, Matei D, Mauritsen T, Mikolajewicz U, Mueller W, Notz D, Pithan F, Raddatz T, Rast S, Redler R, Roeckner E, Schmidt H, Schnur R, Segschneider J, Six KD, Stockhause M, Timmreck C, Wegner J, Widmann H, Wieners KH, Claussen M, Marotzke J, Stevens B (2013) Climate and carbon cycle changes from 1850 to 2100 in MPI-ESM simulations for the Coupled Model Intercomparison Project phase 5. J Adv Model Earth Syst 5(3):572–597. doi:10.1002/jame.20038

Gu G, Adler RF (2012) Interdecadal variability/long-term changes in global precipitation patterns during the past three decades: global warming and/or pacific decadal variability? Clim Dyn 40(11–12):3009–3022. doi:10.1007/s00382-012-1443-8

Hansen J, Ruedy R, Sato M, Lo K (2010) Global surface temperature change. Rev Geophys 48:RG4004. doi:10.1029/2010RG000345

Hunt BG (2008) Secular variation of the Pacific Decadal Oscillation, the North Pacific Oscillation and climatic jumps in a multi-millennial simulation. Clim Dyn 30(5):467–483. doi:10.1007/s00382-007-0307-0

Kaplan A, Cane MA, Kushnir Y, Clement AC, Blumenthal MB, Rajagopalan B (1998) Analyses of global sea surface temperature 1856–1991. J Geophys Res Oceans (1978–2012) 103(C9):18567–18589

Keenlyside NS, Latif M, Jungclaus J, Kornblueh L, Roeckner E (2008) Advancing decadal-scale climate prediction in the north Atlantic sector. Nature 453(7191):84–88. doi:10.1038/nature06921

Kipfmueller KF, Larson ER, George SS (2012) Does proxy uncertainty affect the relations inferred between the pacific decadal oscillation and wildfire activity in the western united states? Geophys Res Lett. doi:10.1029/2011gl050645

Knutson TR, Zeng F, Wittenberg AT (2013) Multimodel assessment of regional surface temperature trends: CMIP3 and CMIP5 twentieth-century simulations. J Clim 26(22):8709–8743

Landrum L, Otto-Bliesner BL, Wahl ER, Conley A, Lawrence PJ, Rosenbloom N, Teng H (2013a) Last millennium climate and its variability in CCSM4. J Clim 26(4):1085–1111. doi:10.1175/jcli-d-11-00326.1

Landrum L, Otto-Bliesner BL, Wahl ER, Conley A, Lawrence PJ, Rosenbloom N, Teng H (2013b) Last millennium climate and its variability in CCSM4. J Clim 26(4):1085–1111. doi:10.1175/jcli-d-11-00326.1

Lavigne F, Degeai JP, Komorowski JC, Guillet S, Robert V, Lahitte P, Oppenheimer C, Stoffel M, Vidal CM, Surono Pratomo I, Wassmer P, Hajdas I, Hadmoko DS, de Belizal E (2013) Source of the great A.D. 1257 mystery eruption unveiled, Samalas volcano, Rinjani volcanic complex, Indonesia. Proc Natl Acad Sci 110(42):16742–16747. doi:10.1073/pnas.1307520110

Livezey RE, Chen WY (1983) Statistical field significance and its determination by monte carlo techniques. Month Weather Rev 111(1):46–59. doi:10.1175/1520-0493(1983)111<0046:SFSAID>2.0.CO;210.1175/1520-0493(1983)111<0046:SFSAID>2.0.CO;2

Lyon B, Barnston AG, DeWitt DG (2013) Tropical pacific forcing of a 1998–1999 climate shift: observational analysis and climate model results for the boreal spring season. Clim Dyn 43(3–4):893–909. doi:10.1007/s00382-013-1891-9

Mantua NJ, Hare SR (2002) The Pacific decadal oscillation. J Oceanogr 58:35–44

Mantua NJ, Hare SR, Zhang Y, Wallace JM, Francis RC (1997) A Pacific interdecadal climate oscillation with impacts on salmon production. Bull Am Meteorol Soc 78:1069–1079

McAfee SA (2014) Consistency and the lack thereof in Pacific decadal oscillation impacts on North American winter climate. J Clim 27(19):7410–7431. doi:10.1175/jcli-d-14-00143.1

McCabe GJ, Palecki MA, Betancourt J (2004a) Pacific and Atlantic Ocean influences on multidecadal drought frequency in the United States. Proc Natl Acad Sci USA 101(12):4136–4141

McCabe GJ, Palecki MA, Betancourt JL (2004b) Pacific and Atlantic Ocean influences on multidecadal drought frequency in the United States. Proc Nat Acad Sci 101(12):4136–4141. doi:10.1073/pnas.0306738101

Meehl GA, Arblaster JM, Branstator G (2012) Mechanisms contributing to the warming hole and the consequent U.S. East–West differential of heat extremes. J Clim 25(18):6394–6408. doi:10.1175/jcli-d-11-00655.1

Meehl GA, Hu A, Arblaster JM, Fasullo J, Trenberth KE (2013) Externally forced and internally generated decadal climate variability associated with the interdecadal pacific oscillation. J Clim 26(18):7298–7310. doi:10.1175/jcli-d-12-00548.1

Minobe S (1997) A 50–70 year climatic oscillation over the North Pacific and North America. Geophys Res Lett 24:683–686

Minobe S (1999) Resonance in bidecadal and pentadecadal climate oscillations over the North Pacific: Role in climatic regime shifts. Geophys Res Lett 26(7):855–858

Neumaier A, Schneider T (2001) Estimation of parameters and eigenmodes of multivariate autoregressive models. ACM Trans Math Softw 27(1):27–57

Newman M, Compo GP, Alexander MA (2003) ENSO-forced variability of the pacific decadal oscillation. J Clim 16(23):3853–3857. doi:10.1175/1520-0442(2003)016<3853:evotpd>2.0.co;210.1175/1520-0442(2003)016<3853:evotpd>2.0.co;2

Park JH, An SI, Yeh SW, Schneider N (2013) Quantitative assessment of the climate components driving the pacific decadal oscillation in climate models. Theor Appl Climatol 112(3–4):431–445

Peterson WT, Schwing FB (2003) A new climate regime in northeast Pacific ecosystems. Geophys Res Lett. doi:10.1029/2003GL017528

Phipps SJ, McGregor HV, Gergis J, Gallant AJE, Neukom R, Stevenson S, Ackerley D, Brown JR, Fischer MJ, van Ommen TD (2013) Paleoclimate data-model comparison and the role of climate forcings over the past 1500 years. J Clim 26(18):6915–6936. doi:10.1175/jcli-d-12-00108.1

Polade SD, Gershunov A, Cayan DR, Dettinger MD, Pierce DW (2013) Natural climate variability and teleconnections to precipitation over the Pacific-North American region in CMIP3 andCMIP5 models. Geophys Res Lett 40(10):2296–2301. doi:10.1002/grl.50491

Priestley MB (1965) Evolutionary spectra and non-stationary processes. J R Stat Soc Ser B (Methodol) 27(2):204–237

Randall DA, Wood RA, Bony S, Colman R, Fichefet T, Fyfe J, Kattsov V, Pitman A, Shukla J, Srinivasan J, Stouffer RJ, Sumi A, Taylor KE (2007) Climate models and their evaluation. In: Solomon S, Qin D, Manning M, Chen Z, Marquis M, Averyt KB, Tignor M, Miller HL (eds) Climate Change 2007: The Physical Science Basis. Contribution of Working Group I to the Fourth Assessment Report of the Intergovernmental Panel on Climate Change

Rayner NA, Parker DE, Horton EB, Folland CK, Alexander LV, Rowell DP, Kent EC, Kaplan A (2003) Global analyses of sea surface temperature, sea ice, and night marine air temperature since the late nineteenth century. J Geophys Res. doi:10.1029/2002jd002670

Rayner NA, Brohan P, Parker DE, Folland CK, Kennedy JJ, Vanicek M, Ansell TJ, Tett SFB (2006) Improved analyses of changes and uncertainties in sea surface temperature measured in situ since the Mid-Nineteenth Century: the HadSST2 dataset. J Clim 19(3):446–469. doi:10.1175/jcli3637.1

Schmidt GA, Jungclaus JH, Ammann CM, Bard E, Braconnot P, Crowley TJ, Delaygue G, Joos F, Krivova NA, Muscheler R, Otto-Bliesner BL, Pongratz J, Shindell DT, Solanki SK, Steinhilber F, Vieira LEA (2011) Climate forcing reconstructions for use in PMIP simulations of the last millennium (v1.0). Geosci Model Dev 4:33–45. doi:10.5194/gmd-4-33-2011

Schmidt GA, Jungclaus JH, Ammann CM, Bard E, Braconnot P, Crowley TJ, Delaygue G, Joos F, Krivova NA, Muscheler R, Otto-Bliesner BL, Pongratz J, Shindell DT, Solanki SK, Steinhilber F, Vieira LEA (2012) Climate forcing reconstructions for use in PMIP simulations of the Last Millennium (v1.1). Geoscientific Model. Development 5(1):185–191

Schmidt GA, Kelley M, Nazarenko L, Ruedy R, Russell GL, Aleinov I, Bauer M, Bauer SE, Bhat MK, Bleck R, Canuto V, Chen YH, Cheng Y, Clune TL, Genio AD, de Fainchtein R, Faluvegi G, Hansen JE, Healy RJ, Kiang NY, Koch D, Lacis AA, LeGrande AN, Lerner J, Lo KK, Matthews EE, Menon S, Miller RL, Oinas V, Oloso AO, Perlwitz JP, Puma MJ, Putman WM, Rind D, Romanou A, Sato M, Shindell DT, Sun S, Syed RA, Tausnev N, Tsigaridis K, Unger N, Voulgarakis A, Yao MS, Zhang J (2014) Configuration and assessment of the GISS ModelE2 contributions to the CMIP5 archive. J Adv Model Earth Syst 6(1):141–184. doi:10.1002/2013ms000265

Schneider N, Cornuelle BD (2005) The forcing of the Pacific decadal oscillation. J Clim 18(21):4355–4373. doi:10.1175/jcli3527.1

Schneider U, Becker A, Finger P, Meyer-Christoffer A, Rudolf B, Ziese M (2011) GPCC Full Data Reanalysis Version 6.0 at 1.0: monthly land-surface precipitation from Rain-Gauges built on GTS-based and historic data. doi:10.5676/DWD_GPCC/FD_M_V6_050

Schneider U, Becker A, Finger P, Meyer-Christoffer A, Ziese M, Rudolf B (2013) GPCC's new land surface precipitation climatology based on quality-controlled in situ data and its role in quantifying the global water cycle. Theor Appl Climatol 115(1–2):15–40. doi:10.1007/s00704-013-0860-x

Sheffield J, Camargo SJ, Fu R, Hu Q, Jiang X, Johnson N, Karnauskas KB, Kim ST, Kinter J, Kumar S, Langenbrunner B, Maloney E, Mariotti A, Meyerson JE, Neelin JD, Nigam S, Pan Z, Ruiz-Barradas A, Seager R, Serra YL, Sun DZ, Wang C, Xie SP, Yu JY,

Zhang T, Zhao M (2013) North american climate in CMIP5 experiments. Part II: evaluation of historical simulations of intraseasonal to decadal variability. J Clim 26(23):9247–9290. doi:10.1175/jcli-d-12-00593.1

Smerdon JE (2011) Climate models as a test bed for climate reconstruction methods: pseudoproxy experiments. Wiley Interdiscip Rev Clim Change 3(1):63–77. doi:10.1002/wcc.149

Smith TM, Reynolds RW, Peterson TC, Lawrimore J (2008) Improvements to NOAA's historical merged land-ocean surface temperature analysis (1880–2006). J Clim 21(10):2283–2296. doi:10.1175/2007jcli2100.1

St. George S, Ault T (2011) Is energetic decadal variability a stable feature of the central Pacific Coast's winter climate? J Geophys Res 116:D12102. doi:10.1029/2010JD015325

Steiger NJ, Hakim GJ, Steig EJ, Battisti DS, Roe GH (2014) Assimilation of time-averaged pseudoproxies for climate reconstruction. J Clim 27(1):426–441. doi:10.1175/jcli-d-12-00693.1

Steinhilber F, Beer J, Fröhlich C (2009) Total solar irradiance during the holocene. Geophys Res Lett. doi:10.1029/2009gl040142

Stoner AMK, Hayhoe K, Wuebbles DJ (2009) Assessing general circulation model simulations of atmospheric teleconnection patterns. J Clim 22(16):4348–4372. doi:10.1175/2009jcli2577.1

Swetnam TW, Betancourt JL (2010) Mesoscale disturbance and ecological response to decadal climatic variability in the American Southwest. In: Tree rings and natural hazards. Springer, Berlin, pp 329–359. doi:10.1007/978-90-481-8736-2_32

Taylor KE, Stouffer RJ, Meehl GA (2012) An overview of CMIP5 and the experiment design. Bull Am Meteorol Soc 93:485–498

Thomson DJ (1982) Spectrum estimation and harmonic analysis. Proc IEEE 70:1055–1096

Tierney JE, Abram NJ, Anchukaitis KJ, Evans MN, Giry C, Kilbourne KH, Saenger CP, Wu HC, Zinke J (2015) Tropical sea surface temperatures for the past four centuries reconstructed from coral archives. Paleoceanography. doi:10.1002/2014PA002717

Vieira LEA, Solanki SK, Krivova NA, Usoskin I (2011) Evolution of the solar irradiance during the Holocene. Astronomy Astrophys. doi:10.1051/0004-6361/201015843

Wang H, Schubert S, Suarez M, Chen J, Hoerling M, Kumar A, Pegion P (2009) Attribution of the seasonality and regionality in climate trends over the United States during 1950–2000. J Clim 22(10):2571–2590. doi:10.1175/2008jcli2359.1

Weaver SJ (2013) Factors associated with decadal variability in great plains summertime surface temperatures. J Clim 26(1):343–350. doi:10.1175/jcli-d-11-00713.1

Wise EK (2014) Tropical Pacific and Northern Hemisphere influences on the coherence of Pacific decadal oscillation reconstructions. Int J Climatol 35(1):154–160. doi:10.1002/joc.3966

Xiao-Ge X, Tong-Wen W, Jiang-Long L, Zai-Zhi W, Wei-Ping L, Fang-Hua W (2012) How well does BCC_CSM1.1 reproduce the 20th century climate change over China? Atmos Ocean Sci Lett 6(1):21–26

Yim BY, Kwon M, Min HS, Kug JS (2015) Pacific decadal oscillation and its relation to the extratropical atmospheric variation in CMIP5. Clim Dyn 44(5–6):1521–1540. doi:10.1007/s00382-014-2349-4

Zanchettin D, Rubino A, Matei D, Bothe O, Jungclaus JH (2012) Multi-decadal-to-centennial SST variability in the MPI-ESM simulation ensemble for the last millennium. Clim Dyn 40(5–6):1301–1318. doi:10.1007/s00382-012-1361-9

Zhang Y, Wallace JM, Battisti DS (1997) ENSO-like interdecadal variability: 1900–93. J Clim 10(5):1004–1020

Zhou T, Li B, Man W, Zhang L, Zhang J (2011) A comparison of the Medieval Warm Period, Little Ice Age and 20th century warming simulated by the FGOALS climate system model. Chin Sci Bull 56(28–29):3028–3041. doi:10.1007/s11434-011-4641-6